

Constitutive Model of Rock, Nonlinearity and Localization

Yu.P. Stefanov^{1,2,*}

¹ Trofimuk Institute of Petroleum Geology and Geophysics SB RAS, Koptug ave. 3, 630090, Novosibirsk, Russia

² Institute of Strength Physics and Materials Science SB RAS, pr. Akademicheskii, 2/4, 634055, Tomsk, Russia

Article history

Received August 28, 2023

Accepted September 09, 2023

Available online September 30, 2023

Abstract

The paper deals with the key features of rock behavior and their manifestations in loading diagrams. Mathematical models are proposed for describing elastic-plastic deformation, creep, and fracture of rocks. Deformation beyond the elastic limit is described using a model based on the combined yield surface and the nonassociated flow rule. The yield surface consists of tension cut-off segment, modified linear segments of the Drucker–Prager criterion and cup. The dilatancy coefficient depends on pressure and volumetric deformation. Model equations are derived to describe deformation in the dilation and compaction modes, as well as strain localization and fracture with consideration for damage kinetics. Several examples of numerical modeling are given to illustrate these phenomena.

Keywords: Rock; Dilatancy; Compaction, Stress; Localization; Constitutive relation

1. INTRODUCTION

The solution of geomechanical problems, like any calculation of stresses and strains in a body, is performed within a mathematical model describing the behavior of the given medium. The main difficulty is that the heterogeneous structure and the presence of pores and cracks of different sizes lead to complex nonlinear behavior of rocks under loading, which strongly depends on the loading scale and conditions. The key factors include the effective stresses, time of the process, temperature, pore pressure, as well as physico-chemical aspects in some cases.

The complex behavior of rocks is observed at all stages of deformation. The early loading stage with reversible deformation corresponds to nonlinear elasticity, associated with the closure of a part of micropores and cracks [1–4]. After reaching the yield point, the hardening stage begins during which the reversible and irreversible parts of deformation increase and the yield limit also increases. Irreversible deformation of rocks can be accompanied by dilation or compaction; its volume either increases or decreases depending on the stress state and structure of rock. Beyond the ultimate stress, shear banding and failure occur. The orientation of macrocracks and shear bands

also depends on the irreversible deformation mode with dilation or compaction.

Other factors influencing the behavior of rocks are the time of the process and the scale. The effect of the sample dimensions is primarily due to the imperfect structure, cracks, macrodefects, and heterogeneities, which cannot be neglected as they largely determine the deformation behavior of the medium. For example, unhealed fault zones are the primary sources of deformation, and heterogeneities lead to nonuniform stress distribution and concentration. The appearance of the time factor even in quasi-static problems is due to a prominent role of dislocation processes, viscous effects, and creep, whose influence increases at long times.

Thus, a number of problems can be identified for describing the behavior of rocks depending on a variety of conditions and properties. For calculations, a mathematical model is needed that takes into account the basic behavior patterns under given conditions. In addition, it is necessary to have effective algorithms and numerical calculation programs implementing mathematical models, as well as changing conditions at external and internal boundaries, including crack edges. Obviously, the choice of a mathematical model and calculation method is determined by the

* Corresponding author: Yu.P. Stefanov, e-mail: yu_st@mail.ru; stefanovyp@ipgg.sbras.ru

specific task. Some cases require the use of coupled poro-elastic-plasticity models that describe the coupled processes of rock mass deformation and diffusion of liquid or heat. There are no universal models and algorithms because their development is too complex and actually ineffective. Therefore, the concept of universality must be used taking into account a particular object and conditions, as well as the possibility of broadening the class of described phenomena and processes that can be potentially important. Clearly, the decisive role in solving a problem is played by the problem formulation and consequently by the choice of a mathematical model, which is based on the interpretation of available data on rock properties and possible behavioral scenarios under given conditions.

Here we present a mathematical model and use it to consider the deformation features of rocks and their manifestations in loading diagrams. The reported results of numerical modeling were obtained using the proposed mathematical model and original software developed by solving dynamic equations with an explicit numerical scheme [5]. Algorithms for 2D and 3D numerical calculations and the implementation of mathematical models are described in more detail elsewhere [6–8].

2. CONSTITUTIVE RELATIONS

Here we adopt the hypothesis that the deformation and the strain rate can be decomposed into elastic and irreversible parts:

$$\dot{\varepsilon}_{ij} = \dot{\varepsilon}_{ij}^e + \dot{\varepsilon}_{ij}^{irr}, \quad (1)$$

where $\dot{\varepsilon}_{ij}$ is the strain rate component, and the irreversible part can also include plastic and viscous components:

$$\dot{\varepsilon}_{ij}^{irr} = \dot{\varepsilon}_{ij}^p + \dot{\varepsilon}_{ij}^v. \quad (2)$$

Then the law of elasticity can be written as:

$$\sigma_{ij} = \lambda (\dot{\varepsilon} - \dot{\varepsilon}^{irr}) \delta_{ij} + 2\mu (\dot{\varepsilon}_{ij} - \dot{\varepsilon}_{ij}^{irr}) \quad (3)$$

where σ_{ij} are the stress tensor components, the dot above means the time derivative, λ and μ are the Lamé parameters and δ_{ij} is the Kronecker delta. Note that the rates of change of stresses and strains in the given equations can be replaced by their increments.

For viscous deformation we write the equation:

$$\dot{\varepsilon}_{ij}^v = \frac{s_{ij}}{\eta}, \quad (4)$$

where s_{ij} are the deviatoric stress tensor components, and η is the viscosity coefficient. The increment of the inelastic or plastic part of the strain tensor, calculated when the stresses reach the yield surface $f(\sigma_{ij}, \varepsilon_{ij}^p) = 0$, is determined by the equation:

$$d\varepsilon_{ij}^p = d\lambda \frac{\partial g}{\partial \sigma_{ij}}, \quad (5)$$

Where $d\varepsilon_{ij}^p$ is the plastic strain increment, $g(\sigma_{ij}, \varepsilon_{ij}^p)$ is the plastic potential, and $d\lambda$ is the multiplier determined during the process. It should be noted that we use the non-associated flow rule, indicating that the plastic potential function and the yield function are independent.

Deformation beyond the elastic limit is described using the combined yield surface [7,8], shown in Fig. 1. The yield surface curve consists of three regions, including two linear segments of the Drucker-Prager failure line [9–12]:

$$f_1 = \tau - \alpha_u \sigma - Y_u, \quad \text{at } \sigma_t \leq \sigma \leq \sigma_u, \quad (6)$$

$$f_2 = \tau - \alpha \sigma - Y, \quad \text{at } \sigma_u < \sigma \leq \sigma_0, \quad (7)$$

and the elliptical cap [13]:

$$f_3 = \frac{(\sigma - \sigma_0)^2}{a^2} + \frac{\tau^2}{b^2} - 1 = 0, \quad \text{at } \sigma > \sigma_0, \quad (8)$$

where $\sigma = -\sigma_{kk}/3$ is the first stress tensor invariant, $\tau = (s_{ij}s_{ij}/2)^{1/2}$ is the equivalent shear stress, α and Y are parameters, and $a = \sigma_1 - \sigma_0$, $b = c + \alpha\sigma_0$ are the semi-axes of the ellipse. The linear form of the Drucker-Prager yield surface is adopted for simplicity, as well as because the generally accepted data contain a minimum of parameters, usually the values of cohesion and internal friction. The presence of junction points between the surface segments

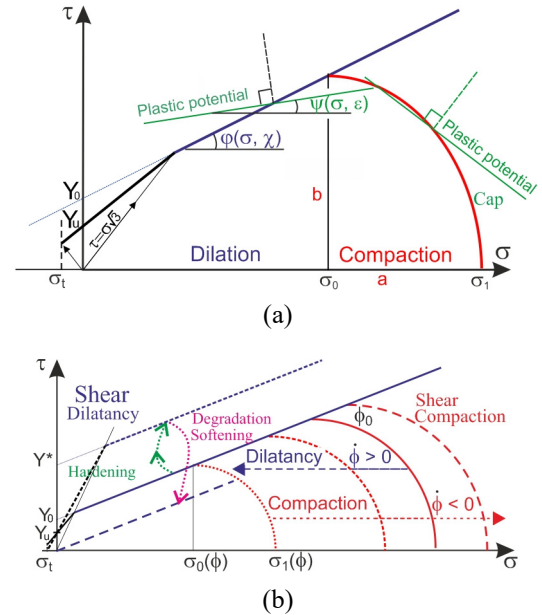


Fig. 1. Generalized view of (a) combined yield surface: τ is the equivalent shear stress, σ are the average stresses, ϕ is the Drucker-Prager internal friction angle, Y_0 is the Drucker-Prager cohesion, σ_0 is the threshold effective pressure of transition from dilation to compaction; (b) changes in the yield surface during inelastic deformation.

is not a problem from the mathematical point of view, because we can accept that these points belong to only one of the segments. It is also easy to slightly modify the equations to ensure a smooth transition between the segments.

Since the Drucker–Prager surface does not describe the behavior of rocks under tensile conditions, a truncated surface is usually used under negative pressure or normal stress. Modeling the deformation and fracture of samples under uniaxial loading encounters great difficulties. Conventional models and approaches do not work. Therefore, either very complicated models are applied, or heterogeneous samples are considered [14,15]. Here this problem was solved with minor changes reflected in Fig. 1 and in the corresponding equations. It is not difficult to ensure a smooth connection of sections using smoothing. Under uniaxial loading, the stress state to the left of the line described by the relation $\tau = \sigma\sqrt{3}$ contains at least one tensile stress component. This means that the yield surface and model must be constrained or corrected from the point of intersection of the given line with the yield surface. The intersection point is determined by the coordinates:

$$\sigma = Y / (\sqrt{3} - \alpha), \quad \tau = Y \left(1 + \frac{\alpha}{\sqrt{3} - \alpha} \right). \quad (9)$$

With available tensile test data, the situation is clear. If there are no such data, it can be assumed that, e.g., $\alpha_u = 2\alpha$, then

$$Y_u = Y \frac{\sqrt{3} - \alpha_u}{\sqrt{3} - \alpha}, \quad \text{where } \alpha_u, \alpha < \sqrt{3}. \quad (10)$$

The initial yield surface corresponds to the elastic limit and describes only the beginning of the process, providing the first estimates of the onset of plastic deformation. Changes in the yield surface during irreversible deformation at the hardening and softening stages are convenient to describe using the equation [6–8,12]:

$$Y(\gamma^p) = Y_0 \left[1 + h(A(\gamma^p) - D(\gamma^p)) \right], \quad (11)$$

where h is the hardening coefficient, $d\gamma^p$ is the increment in the equivalent shear plastic strain, $A(\gamma^p) = 2\gamma^p / \gamma^*$, and $D(\gamma^p) = (\gamma^p / \gamma^*)^2$, γ^* is the critical strain above which the material softening prevails.

Compaction occurs with changes in the yield surface cap, which can shift along the pressure axis and expand. This process can be described by the relation [7,8]:

$$\sigma_0(\varepsilon^p) = \sigma_0 \left(\frac{\varepsilon^*}{\varepsilon^* + \varepsilon^p} \right)^m, \quad (12)$$

equivalent to $\sigma'_0(\phi) = \sigma'_0(\phi^*/\phi)^m$, where $\varepsilon^* = \phi^*$ is the initial porosity, $\Delta\phi = \varepsilon^p$ is the volumetric strain, $a = a_0 + r\Delta\sigma_0$, r

and m are parameters. The plastic potential equations are assumed to take the form [7]:

$$g = \tau - \beta\sigma, \quad \text{for } \sigma \leq \sigma_0, \quad (13)$$

$$g = -\beta_1\sigma + \kappa\tau, \quad \text{for } \sigma > \sigma_0, \quad (14)$$

so that $\beta_1 = \sin\psi$, $\kappa = \cos\psi$, where angle ψ determines the slope of the plastic potential surface, and $\beta_1/\kappa = \beta$,

$$\beta = d\varepsilon^p / d\gamma^p \quad (15)$$

is the dilatancy coefficient. It should be noted that the dilatancy coefficient is the most difficult parameter to determine, because its value strongly depends not only on the initial properties of rock, but also on the current stress-strain state. There are many equations taking into account the stress-strain dependence of the dilatancy coefficient, e.g., [7,11,16–18].

The dilatancy coefficient is usually constrained as $\beta \leq \alpha$, e.g., [11]. By considering the relation of work on plastic strain, it is easy to obtain that for the Drucker–Prager model:

$$\beta < \alpha + \frac{Y}{\sigma}. \quad (16)$$

Therefore, the commonly used constraint is valid in the case of a granular medium. At low pressures in the rock, the dilatancy coefficient can take higher values, which is confirmed by numerical modeling results. With increasing pressure and the development of plastic deformation, the dilatancy coefficient decreases.

The proposed model corresponds to a series connection of elastic, plastic and viscous elements. However, the description of rock deformation often requires a more complicated model that takes into account additional viscoelastic and viscoplastic properties. A schematic of such a model is presented in Fig. 2. The first element in the schematic corresponds to elasticity with modulus μ_1 . The second element corresponds to plasticity and fracture that occur upon reaching the equivalent shear stress τ_{s1} . The third element corresponds to viscosity with coefficient η_1 . The parallel connection of the plastic and viscous elements (Fig.2, element 4) indicates that viscous deformation occurs beyond the elastic limit τ_{s2} . In this case, the irreversible strain increment is determined by the equation:

$$d\varepsilon_{ij}^p = \left(d\lambda \frac{dt}{t^{rel}} \right) \frac{\partial g}{\partial \sigma_{ij}}, \quad (17)$$

where t^{rel} is the relaxation time, dt is time increment.

The last element 5 allows taking into account the influence of the loading rate on the elastic moduli and the velocity dispersion of elastic waves.

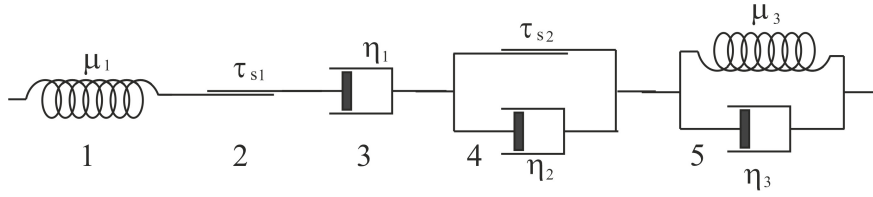


Fig. 2. A mechanical schematic of the rock behavior model.

The time of loading of the medium often greatly affects the deformation process, not only due to creep but also due to crack initiation and growth [15]. Fracture occurs due to damage accumulation in the medium and a decrease in the effective strength. This process can be taken into account using kinetic parameters. The change in strength due to damage accumulation was taken into account by means of the equation:

$$Y(\gamma^p, \sigma, t) = Y_0 \left[1 + h(A(\gamma^p) - D(\gamma^p)) \right] (1 - D'(\sigma, t)) \quad (18)$$

where D' is the kinetic function based on the linear damage accumulation rule:

$$D' = \int_{t_0}^{t^*} \frac{(\Sigma - \Sigma_0)^2}{\Sigma^{*2} T^{*2}} dt. \quad (19)$$

Here Σ , Σ_0 are Coulomb stress (or other effective stress for specific conditions) and the threshold stress above which damage accumulation begins, Σ^* and T^* are the stress and the characteristic time that determine the damage accumulation rate, t_0 and t^* are the initial and current times.

The discussed approach is effective when considering the failure of underground structures with time, karst sink-hole formation, or mine roof collapse, e.g., [19–21]. Fig. 3 shows the process of rock failure with shear banding under its own weight in conditions where stresses do not reach the initial strength of the medium throughout the entire volume.

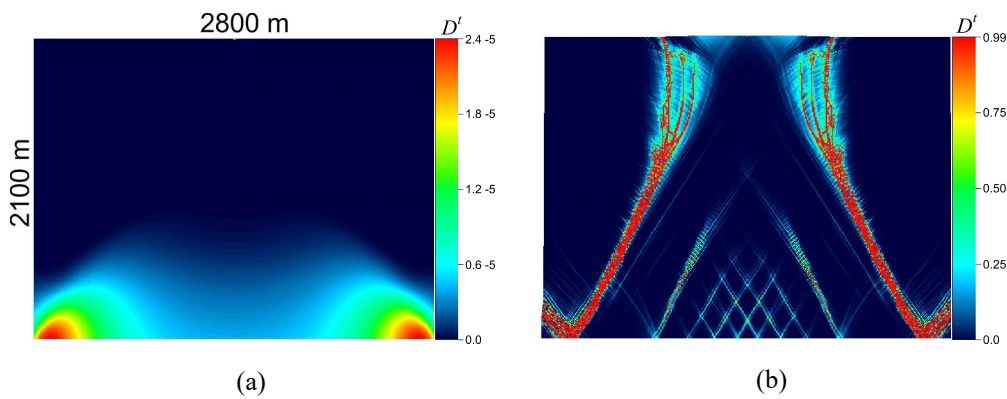


Fig. 3. Shear banding in the rock mass due to long-term damage accumulation under its own weight: (a) 0.1 model period (year); (b) 100 model periods (years).

3. DEFORMATION OF ROCK SAMPLES

The study of rock properties, the construction of behavior models, and the determination of model parameters are carried out on laboratory rock samples with dimensions of several centimeters [1–4]. Therefore, we will first highlight the most important behavior features of rocks on this scale. Analysis of loading diagrams with identifying the characteristic stages of rock deformation in the corresponding curve regions can be found in many works, e.g., [1–4,22]. We will briefly describe, in a simplified form, the most important behavior features and their manifestations in loading diagrams in order to choose a basic behavior model and determine its parameters for numerical calculations.

Fig. 4 shows a generalized view of rock loading diagrams for axial and volumetric strains in different deformation modes, where $Q = \sigma_1 - \sigma_c$. The initial stage of loading curves is often nonlinear, primarily due to multiple mesocracks, some of which are open. As the load increases, the cracks close, and the elastic moduli increase [1,2,23–26]. The value of the deviation from linearity is determined by the crack opening volume, which is closed with loading. Quite simple relations of nonlinear elasticity are proposed in [22,27,28]. Experimental loading curves often have different slopes at different confining pressures. In this case, the pressure dependence of elastic moduli can be constructed without assessing the void volume.

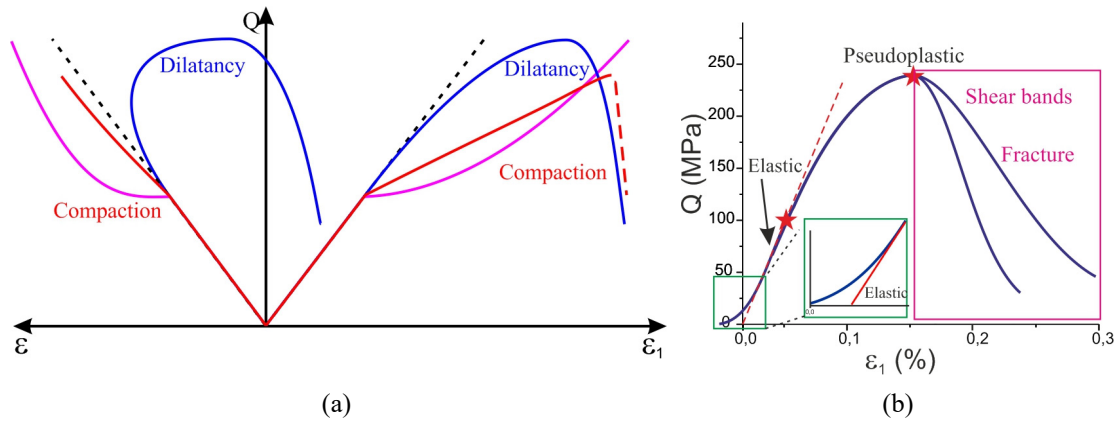


Fig. 4. Characteristic view of rock loading diagrams for axial and volumetric strains.

Deviation from the linear course indicates the beginning of irreversible deformation. This point on the loading diagram, corresponding to the elastic limit, is often determined very approximately because the curves are rarely perfect. To identify the point, it is necessary to consider not only the axial strain curves, but also radial and volumetric ones. The volumetric strain curve often shows more clearly the deviation from the linear elastic portion. The error in determining the elastic limit is partly compensated by taking into account strain hardening.

The main interesting feature in the next loading stage, in addition to the relationship between hardening and accumulated strain, is the ratio of the volumetric and shear components of irreversible deformation. This ratio determines the parameter characterizing dilatancy. As can be seen in the Fig. 4, the deviation from the elasticity portion in the volumetric strain curve can have a different sign, depending on the dilation or compaction mode [29–33]. In the case of dilatancy, the curve bends towards lower compression values as the material expands; the dilation compensates the elastic compression and then exceeds it. As a result, the loading curve turns downward/upward until the initial volume is exceeded. In the case of compaction, on the contrary, the volume decreases rapidly. Therefore, this process must be described by slightly different laws, because the degree of compaction is limited by the presence of pores or voids, and the degree of dilatancy is limited only by maintaining conditional continuity, i.e., the integrity of the studied material, under given conditions. Moreover, when the sample is unloaded and removed from the loading device, it can fragment or even break into pieces.

The important point here is that irreversible deformation proceeds uniformly only in the hardening region, although detailed examination often reveals strain localization zones and internal cracks from the very beginning of deformation. After reaching the ultimate strength, the loading curve usually descends. This stage of deformation is called softening due to a decrease in strength. The stress

often drops sharply at low confining pressure, indicating the formation of main cracks, brittle fracture, and sample breaking. With increasing confining pressure, the descending branch becomes less steep and longer, and fracture occurs in a shear band or a set of bands. In this case, the sample can maintain its conditional integrity and residual strength due to friction between fragments for a long time. In the limiting case of high confining pressure, the behavior is viscous; the stress does not drop or decreases very slowly. However, the descending postcritical branch of the loading diagram no longer indicates the strength decrease, but rather the localization of the process and active damage accumulation in the localization zone.

There are two more differences in the behavior of rock samples in the dilation and compaction modes, which appear in the loading diagrams. During dilatancy the stress usually increases to the ultimate strength and then drops, while compaction occurs with stress increase. The stress drop is possible only under active shear failure with a local reduction in porosity. Noteworthy is that compaction banding appears as the flattest region in the loading diagram and is often accompanied by stress drops [7,29–33]. The more extended and pronounced the flat portion, the more pronounced are the compaction bands. This process is most often observed at the beginning of irreversible deformation when the rock porosity is the highest.

The next difference is reflected in the orientation of strain localization bands, determined by the internal friction and dilatancy coefficients [34–37] and by the stress state. Approximate estimates of the orientation with respect to the principal stress axes are given by the expression [38, 39]: $\theta = 45 + (\varphi + \psi) / 4$, where φ and ψ are the angles of internal friction and dilatancy, respectively. The bands are oriented away from the axis of greatest compression in the range of $0^\circ - 45^\circ$ in the dilation mode and $45^\circ - 90^\circ$ in compaction. Accurately predicting the orientation of strain localization bands is quite difficult, because the parameters change during the process and the

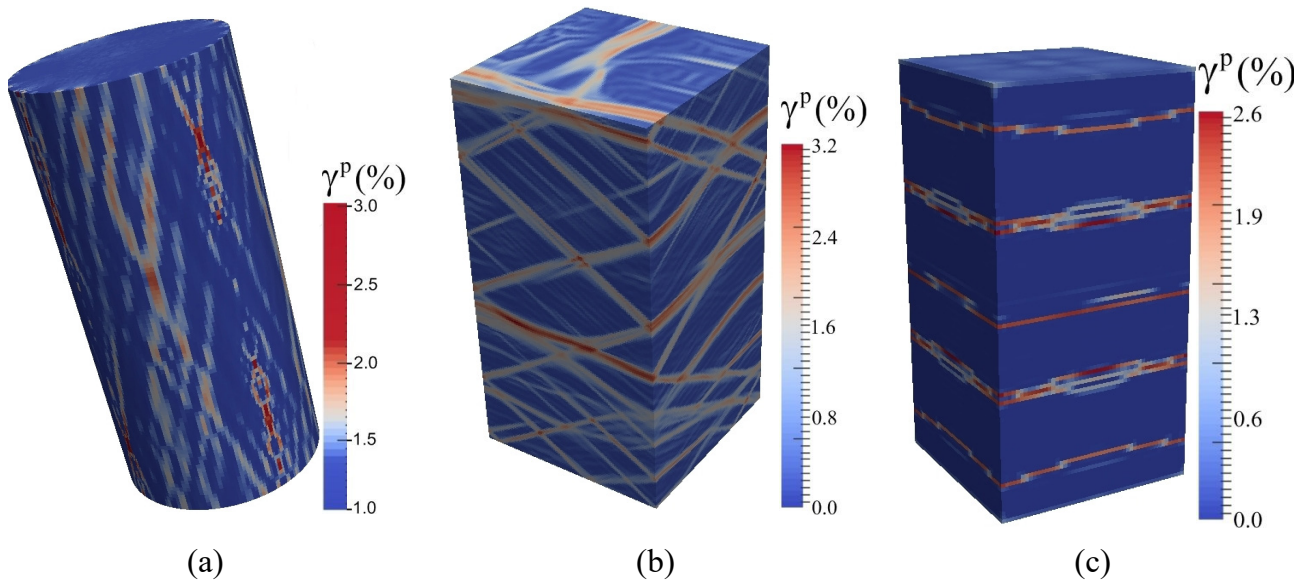


Fig. 5. Numerical calculation of sample deformation. Strain distributions at the stage of shear and compaction bands formation: (a) bazhenov rock under uniaxial loading, (b) sandstone at the confining pressure 60 MPa and (c) 90 MPa.

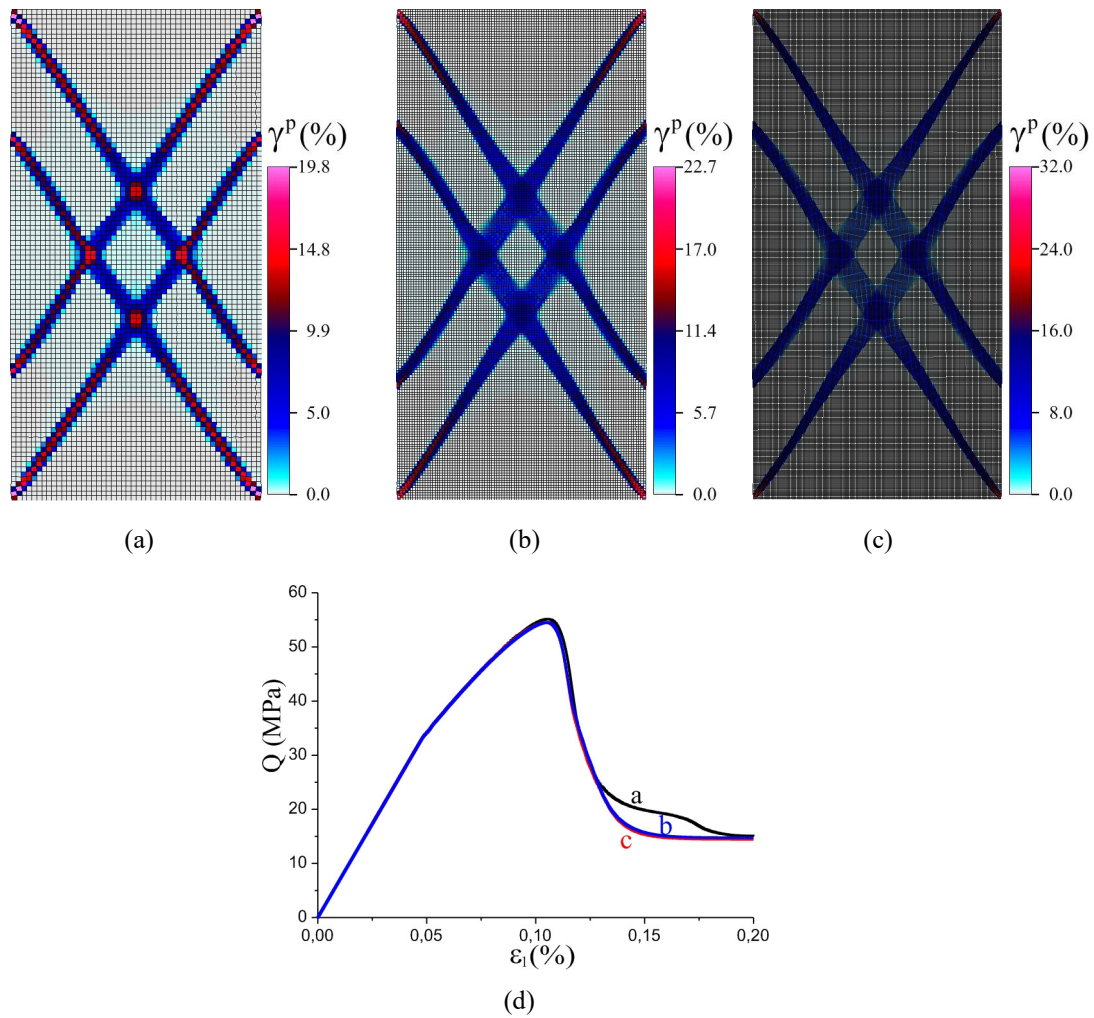


Fig. 6. Convergence of the model solution for shear banding. Calculations on (a) 50×100, (b) 100×200, (c) 200×400 grids and (d) load diagrams.

orientation of the principal stress axes depends on the geometry and can also change in time and space. Fig. 5 shows the numerical modeling results for sample deformation obtained with the proposed model equations under different loading conditions. The Fig. 5 shows the distribution of irreversible strains at the stage of shear banding under uniaxial loading (Fig. 5a) and compaction banding under confining pressures of 60 and 90 MPa (Figs. 5b and 5c). It is clearly seen that in the absence of confining pressure the strain localization bands have an orientation close to the loading axis. At high confining pressure, the orientation of the compaction bands is close to orthogonal with respect to the axis of greatest compression.

Analysis of postcritical deformation at the softening stage and numerical modeling of the unstable process involve significant difficulties [1–4,37–44]. The stress drop rate is determined by the rock properties and the width of localization bands, which in turn depends on the loading conditions and confining pressure. In numerical modeling of the localization process, convergence can be attained by using special models and regularizing algorithms [41–44]. Since the fracture process occurs in time and is dynamic, it can be best described by dynamic equations. However, even in this case, convergence is achieved by using the viscoelastic model element with the relaxation time governing the band width. The relaxation time in Eq. (10) can be specified by the relation $t^{rel} = H / V_s$, where H is the shear band width, and V_s is the shear wave velocity. Thus, the description of the basic features of rock deformation should be based on the model schematized in Fig. 2. An example of numerical calculation using the given equations is shown in Fig. 6. Good agreement is observed between the pattern and thickness of shear bands calculated on different grids.

4. CONCLUSIONS

The behavior of rocks is associated with structural heterogeneity, porosity, and multiple micro-/mesocracks. These structural features determine the specific deformation behavior beyond the elastic limit, as well as nonlinear behavior patterns at all deformation stages. In this work, some nonlinear deformation features were analyzed with a focus on the effects produced by the opening and closing of mesocracks, both preexisting and formed during loading, as well as on the processes induced by long-term loading. Attention was also drawn to the need of taking into account rheological and kinetic parameters.

The considered nonlinear features of rock deformation can play a significant role in solving many geomechanical problems. Though being simple, the proposed equations can take into account many behavioral features of rocks with different porosity.

ACKNOWLEDGEMENTS

The research was supported by the Fundamental Research Program of the State Academies of Sciences for 2022–2025 FWZZ-2022-0021.

REFERENCES

- [1] J.C. Jaeger, N.G.W. Cook, R.W. Zimmerman, *Fundamentals of Rock Mechanics, 4th Edition*, Wiley-Blackwell Publishing, London, 2007.
- [2] C. Fairhurst, *Laboratory measurement of some physical properties of rock*, Proceeding of the 4th Symposium on Rock Mechanics, University Park, Pennsylvania, 1961, pp. 105–118.
- [3] Z.T. Bieniawski, *Mechanism of brittle fracture of rock: Part II—experimental studies // International Journal of Rock Mechanics and Mining Sciences & Geomechanics Abstracts*, 1967, vol. 4, no. 4, pp. 407–423.
- [4] A.N. Stavrogin, B. Tarasov, *Experimental Physics and Rock Mechanics: Results of Laboratory Studies*, Lisse, Abington, 2001.
- [5] M.L. Wilkins, *Computer simulation of dynamic phenomena*, Springer-Verlag, Berlin, 1999.
- [6] Yu.P. Stefanov, R.A. Bakeev, *Formation of Flower Structures in a Geological Layer at a Strike-Slip Displacement in the Basement*, *Izvestiya, Physics of the Solid Earth*, 2015, vol. 51, pp. 535–547.
- [7] Yu.P. Stefanov, M.A. Chertov, G.R. Aidagulov, A.V. Myasnikov, *Dynamics of inelastic deformation of porous rocks and formation of localized compaction zones studied by numerical modeling*, *Journal of the Mechanics and Physics of Solids*, 2011, vol. 59, no. 11, pp. 2323–2340.
- [8] A. Garavand, Yu.P. Stefanov, Y.L. Rebetsky, R.A. Bakeev, A.V. Myasnikov, *Numerical modeling of plastic deformation and failure around a wellbore in compaction and dilation modes*, *International Journal for Numerical and Analytical Methods in Geomechanics*, 2020, vol. 44, no. 6, pp. 823–850.
- [9] D.C. Drucker, W. Prager, *Soil mechanics and plastic analysis or limit design*, *Quarterly of Applied Mathematics*, 1952, vol. 10, pp. 157–165.
- [10] V.N. Nikolaevskii, *Governing equations of plastic deformation of a granular medium*, *Journal of Applied Mathematics and Mechanics*, 1971, vol. 35, no. 6, pp. 1017–1029.
- [11] I.A. Garagash, V.N. Nikolaevskii, *Nonassociated Flow Rules and Localization of Plastic Deformation*, *Uspekhi Mekhaniki*, 1989, vol. 12, pp. 131–183 (in Russian).
- [12] Yu.P. Stefanov, *Deformation localization and fracture of geomaterials: Numerical modeling*, *Physical Mesomechanics*, 2002, vol. 5, no. 5, pp. 107–118.
- [13] E. Grueschow, J.W. Rudnicki, *Elliptic yield cap constitutive modeling for high porosity sandstone*, *International Journal of Solids and Structures*, 2005, vol. 42, no. 16–17, art. no. 4574–4587.
- [14] M.O. Eremin, V.A. Zimina, A.S. Kulkov, Y.P. Stefanov, *Microstructure-Based Computational Analysis of Deformation Stages of Rock-like Sandy-Cement Samples in Uniaxial Compression Materials*, *Materials*, 2023, vol. 16, no. 1, art. no. 24.

- [15] V. Lyakhovskiy, I. Panteleev, E. Shalev, J. Browning, T.M. Mitchell, D. Healy, P.G. Meredith, *A new anisotropic poroelasticity model to describe damage accumulation during cyclic triaxial loading rock*, Geophysical Journal International, 2022, vol. 230, no. 1, pp. 179–201.
- [16] S.M. Kapustyanskii, V.N. Nikolaevskii, A.G. Zhilenkov, *Nonholonomic model of deformation of highly porous sandstone under its internal crushing*, Izvestiya, Physics of the Solid Earth, 2010, vol. 46, pp. 1095–1104.
- [17] B.V. Zamyshlyayev, L.S. Evtarev, *The Models of Dynamic Deformation and Destruction of Ground Media*, Nauka, Moscow, 1990 (in Russian).
- [18] V. Lyakhovskiy, Z. Reches, R. Weinberger, T.E. Scott, *Non-linear elastic behaviour of damaged rocks*, Geophysical Journal International, 1997, vol. 130, no. 1, pp. 157–166.
- [19] R.A. Bakeev, Yu.P. Stefanov, A.A. Duchkov, A.V. Myasnikov, *Modeling of karst deformation and analysis of acoustic emission during sinkhole formation*, AIP Conference Proceedings, 2017, vol. 1909, no. 1, art. no. 020009.
- [20] M. Eremin, G. Esterhuizen, I. Smolin, *Numerical simulation of roof cavings in several Kuzbass mines using finite-difference continuum damage mechanics approach*, International Journal of Mining Science and Technology, 2020, vol. 30, no. 2, pp. 157–166.
- [21] M.O. Eremin, P.V. Makarov, *Mathematical Modeling of Stress-Strain Evolution in the Rock Mass around a Mine Opening. Evaluation of the Steps of First Roof Caving at Different Thicknesses of the Main Roof*, Physical Mesomechanics, 2019, vol. 22, no. 4, pp. 287–295.
- [22] Yu.P. Stefanov, *Some Nonlinear Rock Behavior Effects*, Physical Mesomechanics, 2018, vol. 21, no. 3, pp. 234–241.
- [23] M.J. Heap, S. Vinciguerra, P.G. Meredith, *The evolution of elastic moduli with increasing crack damage during cyclic stressing of a basalt from Mt. Etna volcano*, Tectonophysics, 2009, vol. 471, no. 1–2, pp. 153–160.
- [24] M.L. Kachanov, *Effective elastic properties of cracked solids; critical review of some basic concepts*, Applied Mechanics Reviews, 1992, vol. 45, no. 8, pp. 304–335.
- [25] F.K. Lehner, M. Kachanov, *On the stress-strain relation for cracked elastic materials in compression*, in: *Mechanics of Jointed and Faulted Rock*, ed. by H.-P. Rossmanith, Balkema, Rotterdam, 1995, pp. 49–62.
- [26] A. Nur, G. Simmons, *The origin of small cracks in igneous rocks* // International Journal of Rock Mechanics and Mining Sciences & Geomechanics Abstracts, 1970, vol. 7, no. 3, pp. 307–314.
- [27] Yu.P. Stefanov, A.S. Romanov, R.A. Bakeev, *Effect of Nonlinear Elasticity on Loading Diagrams of Rock Specimens*, AIP Conference Proceedings, 2019, vol. 2167, no. 1, art. no. 020349.
- [28] Y.P. Stefanov, D.K. Zharasbaeva, *Loading diagrams and parameters of the model of elastic-pseudoplastic deformation of black shale rocks of the Bazhenov formation*, Russian Journal of Geophysical Technologies, 2022, no. 3, pp. 13–24 (in Russian).
- [29] R.J. Cuss, E.H. Rutter, R.F. Holloway, *The application of critical state soil mechanics to the mechanical behavior of porous sandstones*, International Journal of Rock Mechanics and Mining Sciences, 2003, vol. 40, no. 6, pp. 847–862.
- [30] H. Fossen, R.A. Schultz, Z.K. Shipton, K. Mair, *Deformation bands in sandstone: a review*, Journal of the Geological Society, 2007, vol. 164, no. 4, pp. 755–769.
- [31] W. Zhu, T. Wong, *The transition from brittle faulting to cataclastic flow. Permeability evolution*, Journal of Geophysical Research, 1997, vol. 102, no. B2, pp. 3027–3041.
- [32] P. Baud, V. Vajdova, T. Wong, *Shear-enhanced compaction and strain localization: Inelastic deformation and constitutive modeling of four porous sandstones*, Journal of Geophysical Research, 2006, vol. 111, no. B12, art. no. B12401.
- [33] W.A. Olsson, *Theoretical and experimental investigation of compaction bands in porous rock*, Journal of Geophysical Research, 1999, vol. 104, no. B4, pp. 7219–7228.
- [34] K.A. Issen, J.W. Rudnicki, *Conditions for compaction bands in porous rock*, Journal of Geophysical Research, 2000, vol. 105, no. B9, pp. 21529–21536.
- [35] J.W. Rudnicki, J.R. Rice, *Condition for localization of plastic deformation in pressure sensitive dilatant materials*, Journal of the Mechanics and Physics of Solids, 1975, vol. 23, no. 6, pp. 371–390.
- [36] I.A. Garagash, *Conditions of the formation of regular systems of shear and compaction bands*, Russian Geology and Geophysics, 2006, vol. 47, no. 5, pp. 657–668.
- [37] A.I. Chemenda, *The formation of shear-band/fracture networks from a constitutive instability: Theory and numerical experiment*, Journal of Geophysical Research, 2007, vol. 112, no. B11, art. no. B11404.
- [38] I. Vardoulakis, *Shear-band inclination and shear modulus of sand in biaxial tests*, International Journal for Numerical and Analytical Methods in Geomechanics, 1980, vol. 4, no. 2, pp. 103–119.
- [39] P.A. Vermeer, R. de Borst, *Non-Associated Plasticity for Soils, Concrete and Rock*, Heron, 1984, vol. 29, no. 3, pp. 1–64.
- [40] A.I. Chemenda, J. Lamarche, C. Matonti, L. Bazalgette, P. Richard, *Origin of Strong Nonlinear Dependence of Fracture (Joint) Spacing on Bed Thickness in Layered Rocks Mechanical Analysis and Modeling*, Journal of Geophysical Research, 2021, vol. 126, no. 3, art. no. e2020JB020656.
- [41] J.H. Prevost, B. Loret, *Dynamic strain localization in elasto-(visco-)plastic solids, part 2. Plane strain examples*, Computer Methods in Applied Mechanics and Engineering, 1990, vol. 83, no. 3, pp. 275–294.
- [42] V.D. Silva, *A simple model for viscous regularization of elasto-plastic constitutive laws with softening*, Communications in Numerical Methods in Engineering, 2004, vol. 20, no. 7, pp. 547–568.
- [43] T. Duretz, R. de Borst, L. Le Pourhiet, *Finite thickness of shear bands in frictional viscoplasticity and implications for lithosphere dynamics*, Geochemistry, Geophysics, Geosystems, 2019, vol. 20, no. 11, pp. 5598–5616.
- [44] R. Borst, T. Duretz, *On viscoplastic regularisation of strain-softening rocks and soils*, International Journal for Numerical and Analytical Methods in Geomechanics, 2020, vol. 44, no. 6, pp. 890–903.

УДК 539.21:539.3:539.4

Модель поведения горных пород, нелинейность и локализация

Ю.П. Стефанов^{1,2}

¹ Институт нефтегазовой геологии и геофизики им. А.А. Трофимука Сибирского отделения Российской академии наук (ИНГГ СО РАН), пр. Академика Коптюга, 3, Новосибирск, 630090, Россия

² Институт физики прочности и материаловедения Сибирского отделения Российской академии наук (ИФПМ СО РАН), Академический пр., 2/4, Томск, 634055, Россия

Аннотация. Рассмотрены важнейшие особенности поведения горных пород и их проявления на диаграммах нагружения. Представлены варианты математических моделей, описывающие упругопластическую деформацию, а также ползучесть и формирование полос локализации. Описание деформации за пределом упругости осуществляется с помощью модели, основанной на комбинированной предельной поверхности и неассоциированном законе течения. Предельная поверхность включает участки модифицированной поверхности Друккера–Прагера и эллиптической зоны. Коэффициент дилатансии зависит от давления и объемной деформации. Предложенные соотношения модели позволяют описывать развитие деформации в режимах дилатансии и компакция, а также локализацию деформации и разрушение с учетом кинетики повреждений. Приведен ряд примеров численного моделирования с иллюстрацией указанных явлений.

Ключевые слова: горные породы; дилатансия; компакция; локализация; определяющие соотношения